DOI: 10.1021/ma1001996

Macromolecules
ARTICLE

# NMR Imaging of Water Uptake in Multilayer Polymeric Films: Stressing the Role of Mechanical Stress

**Viktor Baukh,[†] Hendrik P. Huinink,*[,†] Olaf C. G. Adan,[†,‡] Sebastiaan J. F. Erich,[†,‡] and Leendert G. J. van der Ven[†,§]**

[†]*Department of Applied Physics, Eindhoven University of Technology, P.O. Box 513, NL-5600MB, Eindhoven, The Netherlands,* [‡]*TNO Built Environment and Geosciences, Delft, The Netherlands, and* [§]*AkzoNobel Car Refinishes, Sassenheim, The Netherlands*

*Received January 26, 2010; Revised Manuscript Received March 25, 2010*

ABSTRACT: The penetration of water into two-layer polymeric films of a hydrophilic base layer and hydrophobic top layer plays an important role in their performance. Little is known about the coupled effects of water uptake and stress in such films. To study such interactive phenomena, time-dependent distributions in the film are needed, which cannot be provided by traditional techniques. In this study, high-resolution NMR imaging was used to measure water profiles, showing that applied stress increased both the uptake rate and the amount of absorbed water. A model was formulated to describe the process, using the barrier properties of and the chemical potential differences over the top coat. On the basis of this, the diffusivity in the top layer and stress contribution were estimated. The results show that external stresses significantly influence water penetration into multilayer films.

## Introduction

Organic films play an important role in protecting substrates against deterioration and providing the desired appearance of the substrate. Mostly, they are composed of several layers, with each of them having a specific function. The top coat normally has a barrier function, protecting the substrate from weathering and giving a glossy appearance, whereas underlying layers such as a base coat and primer define the color or introduce functions like corrosion protection and adhesion, respectively.

The penetration of water into organic films plays a pivotal role in the performance of the coating and the degradation of the coated substrate. Although there are numerous studies dedicated to the presence of water in single-layer organic coatings and polymeric films,[1] only a few studies on water transport in multilayer systems have been reported in the literature.[2−5]

Carbonini et al.[2] studied the effects of the chemical composition of the constituent layers on the water uptake in a multilayer system. Both water absorption and degradation depend on the chemical characteristics of each layer but, moreover, also depend on the layer position in the system.[3] Devasahayam[5] has studied an adhesion failure due to permeation of water at different temperatures in multilayer metal-coating systems. It was shown that a combination of parameters like the $T_g$ of the layers and the pigment concentration governs the whole water diffusion through the system. In a recent study, Allahar et al.[4] pointed out that the layer interface can play an important role in the transport of water in multilayer coatings.

It becomes even more complex when mechanical stresses are considered. Water penetration into polymeric films may introduce mechanical response, which in turn may interact with water transport processes in the film. Only few studies are known that address these coupled phenomena, for example, Fahmy and Hurt[6] and Weitsman.[7]

*To whom correspondence should be addressed. E-mail: h.p.huinink@tue.nl.

In conclusion, the documented studies into water uptake in multilayer polymer films show that this complex process cannot be understood on the basis of uptake in single-layer systems.

Until now, the lack of adequate experimental techniques clearly hampered a full understanding of the complex phenomena mentioned above. Various techniques have been and are still being used to probe water uptake by coatings and polymeric films, such as gravimetry, electrochemical impedance spectroscopy,[2−4,8,9] Fourier transform infrared spectroscopy,[10−12] and fluorescence spectroscopy.[13] These techniques only provide information about the total amount of water in a sample, except for Fourier transform infrared spectroscopy, which can be used to probe distribution of water in the direction parallel to the coating/substrate interface.[11,12] A step forward can only be made if the measuring technique features in depth probing with high resolution as a function of time. The only experimental technique that fulfills this requirement is NMR imaging on the basis of the so-called GARfield approach.[14] It proved to be a powerful tool to monitor various processes in not-transparant films with high spatial resolution.[15−18] With the GARfield approach, NMR imaging can be used to measure depth profiles with spatial resolution of $\sim 5\ \mu$m.

The present article focuses on the interaction between mechanical stress and water uptake in a two-layered polymeric system, consisting of a waterborne base layer and a solvent-borne top coat. It uses high-resolution NMR imaging as the key technique to depict both time-dependent water distribution and swelling. This laid the foundation for a better understanding of the barrier function of the upper layer and the driving forces behind the water uptake process in multilayer polymer films.

## Experimental Details

**Nuclear Magnetic Resonance Principles and Setup.** Nuclear magnetic resonance is based on the fact that nuclei in a magnetic field resonate at a specific resonance frequency and can be excited by a radio frequency (RF) pulse. The resonance frequency depends linearly on the magnitude of the applied

 Published on Web 03/31/2010 

magnetic field

$$f = \frac{\gamma}{2\pi}|\vec{B}| \quad (1)$$

where $\gamma/2\pi = 42.58$ (MHz/T) is the gyromagnetic ratio, $|\vec{B}|$ (T) is the magnitude of the applied magnetic field, and $f$ (MHz) is the resonance frequency.

For imaging with NMR, the resonance frequency, $f$, and the magnitude of the magnetic field, $|\vec{B}|$, should be position-dependent. In this study, the GARField approach was used to obtain high-resolution depth profiles.[14] Special shaped magnet poles were used to generate a magnetic field with a high static gradient. In the region of interest, the magnetic field varies linearly with the position $|\vec{B}| = B_0 + Gx$, where $G = \partial|\vec{B}|/\partial x$ denotes the gradient of the absolute value of the magnetic field and $x$ is the direction perpendicular to the coating layer.[14]

The sum of the magnetic moments of the nuclei equals the total magnetization $|\vec{M}|$, which is aligned with the magnetic field, $|\vec{B}|$. During the measurement, the magnetization, $|\vec{M}|$, is flipped to the transversal plane with an RF pulse. The signal is received at $t_e$ (s) after excitation and is proportional to the magnitude of the transversal magnetization. The signal is divided by the signal of an aqueous $CuSO_4$ solution to remove effects of the coil sensitivity and excitation profile. The resulting signal is described by the following equation

$$S_n(x) = \frac{\rho(x)}{\rho_w}[1 - \exp(-t_r/T_1)]\exp(-nt_e/T_2) \quad (2)$$

where $\rho$ (mol/m$^3$) is actual density of probed $^1$H nuclei, $\rho_w$ (mol/m$^3$) is the density of $^1$H nuclei in liquid water, $t_r$ (s) is the repetition time, $T_1$ (s) is the longitudinal relaxation time, $t_e$ (s) is the echo time, $T_2$ (s) is the transversal relaxation time, and $n$ is the number of spin−echo. For imaging the first spin−echoes ($n = 1$) were used.

In general, the $T_2$ relaxation time of nuclei in polymers depends on the mobility of the polymer molecules. When polymer molecules become more mobile, the $T_2$ time increases,[19] for example, if the polymer makes a transition from a glassy to a rubbery state.

In our setup, the magnetic field, $B_0$, equals 1.5 T, and the gradient, $G$, equals 45 T/m. Profiles were measured by using an Ostroff−Waugh pulse sequence $90_x - t_e/2 - [90_y - t_e/2 - \text{echo} - t_e/2]_n$.[20] The duration of a single pulse equals 1 $\mu$s. Because a static gradient is used, the effective field of view (FOV) is determined by both the receiver bandwidth and the spectral content of the RF excitation pulse. Pulses with rise and fall times of roughly 0.25 $\mu$s and duration of 1 $\mu$s were applied, yielding an excitation profile with a thickness of ~500 $\mu$m. The NMR signal was sampled with a frequency of 5 MHz at a receiver bandwidth of 1.5 MHz, resulting in an FOV that is slightly larger than the excitation profile. To obtain the distribution of water, signal profiles were measured with $t_e = 100$ $\mu$s and an acquisition window of 90 $\mu$s, corresponding to a resolution of 6 $\mu$m. Signal profiles with $t_e = 200$ ms, an acquisition window of 190 ms, and a resolution of about 2.5 $\mu$m were measured to obtain more accurate information about the swelling of the samples. Signal profiles were averaged 2048 times, and the time between two subsequent measurements has been set to $t_r = 0.5$ s. A measurement of a single profile measurement took 20 min, and the temporal resolution was 40 min. Home-built NMR equipment was used with acquisition systems described by Kopinga and Pel.[21]

**Sample Description.** The investigated polymeric systems are two-layered base coat/top coat systems. The base coat consists of acrylic particles, DPP (diketo-pyrrolo-pyrrole) pigment particles and polyurethane particles, in weight fractions of 0.45, 0.3, and 0.25, respectively. The acrylic particles are core/shell particles with a hydrophobic core and a hydrophilic shell. The shell/core volume ratio is approximately 1:7. The shell contains methacrylic acid. The glass-transition temperatures, $T_g$, of the polyurethane and acrylic particles are approximately equal to 0 and 20 °C, respectively.

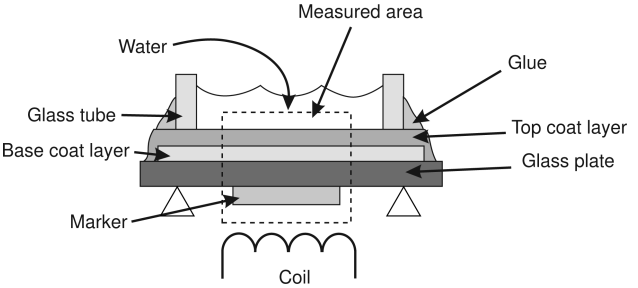


**Figure 1.** Schematic presentation of the experimental setup used in the water uptake experiments.

**Table 1. List of Samples Used for Water Uptake Experiments**[a]

| sample | BC thickness ($\mu$m) | TC thickness ($\mu$m) | glue |
|---|---|---|---|
| BC38/TC23E | 38 ± 3 | 23 ± 2 | epoxy-amine |
| BC40/TC54E | 40 ± 2 | 54 ± 2 | epoxy-amine |
| BC49/TC23E | 49 ± 2 | 23 ± 2 | epoxy-amine |
| BC38/TC23S | 38 ± 3 | 23 ± 2 | silicone |

[a] Letters BC and TC refer to the base coat and top coat, respectively. The numbers added to BC and TC represent the thickness of the layers in micrometers. E and S refer epoxy-amine and silicone glue, respectively.

The top coat is a two-component solvent-borne acrylic polyurethane clearcoat. The glass-transition temperature of the top coat is ~60 °C.

The coatings were applied on glass coverslips with an area of $18 \times 18$ mm$^2$ and a thickness of 150 $\mu$m. The base coat was applied by spraying an aqueous dispersion on the glass slides. After spraying, the base coat was dried at 60 °C for 1 h. The top coat was sprayed on top of the base coat and then cured at 60 °C for ~20 min. To ensure that the samples were fully cured before being used in experiments, the samples were stored for at least 4 weeks at room temperature. It is expected that the base coats are more sensitive to water that the top coat because it is known that water diffuses faster in physical drying systems than in cured systems.[22]

The experimental setup is shown in Figure 1. A glass tube was glued on top of the coating and filled with water to moisten the sample. A marker was fixed at the bottom of the substrate to trace deflections of the substrate and fluctuations of the setup because of instabilities. Those marker shifts were not a consequence of misalignment, which was excluded by checking the slope of the marker/glass interface. This slope did not broaden in the experiments.

Two different types of glue were used to fix the glass tube on the coating surface: an epoxy-amine two-component glue and a silicon glue, respectively. The epoxy-amine glue was cured for at least 1 h before starting water uptake experiments, and the silicon glue was cured for at least 1 day, both under room conditions.

The application of two different types of glue introduced a simple and effective mechanism to induce mechanical stress on the sample within the small space that was available in the NMR insert. The interaction of water with the epoxy-amine glue caused a mechanical response of the glass slide, which was absent when the silicon glue was used.

Our study addressed different combinations of base coat and top coat thicknesses as presented in Table 1. The thicknesses of the samples were determined from cross sections of the samples by using optical microscopy. The sample at which the glass tube was fixated with silicone glue (BC38/TC23S) served as a reference sample because no externally applied stress was present.

Uptake experiments were carried out in two steps. First, a dry sample was measured to obtain the signal profile of the sample in the initial state. Second, after placing water in the tube, the uptake process measurement was started. Next, to the signal profiles, $T_1$ relaxation times were measured for the dry and wet samples. The values are shown in Table 2.

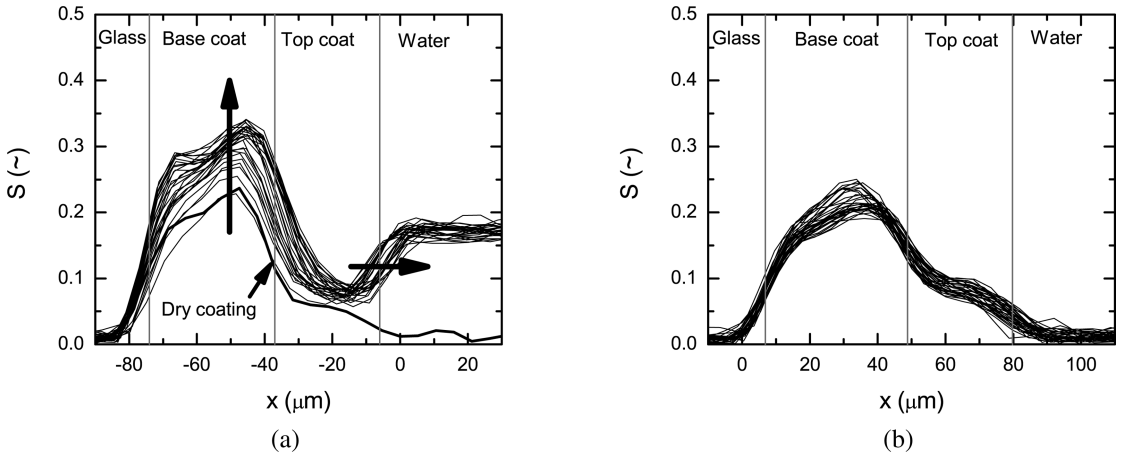


**Figure 2.** NMR signal profiles in the sample BC38TC23E during (a) water and (b) heavy water uptake. The time between subsequent profiles is 40 min and 4 h for the first 10 and the rest of the profiles, respectively. The vertical lines refer to the positions of the interfaces. The vertical arrow denotes the signal increase in the base coat and the horizontal arrow denote swelling. The lower bold line represents the dry sample signal profile.

**Table 2. $T_1$ Values of the Polymer Systems and Water**

| layer/state | $T_1$ (ms) |
|---|---|
| base coat/dry | 200 |
| base coat/wet | 200 |
| top coat/dry | 350 |
| water | 3000 |

Furthermore, a gravimetric determination of the water solubility in the top coat was carried out with a Mettler-Toledo AX205DR analytical balance. A single top coat layer was immersed in water for 1 week and, subsequently, the approximate equilibrium concentration of water in the top coat was measured: $\rho_s \simeq (1.4 \pm 0.4) \times 10^3$ mol/m$^3$.

## Results

**Signal Profiles and Water Distribution during Water Uptake.** This section focuses on the relationship between the NMR signal profiles and the distribution of water in a coating.

The signal profiles of the sample BC38/TC23E are presented in Figure 2a. The profiles as shown were corrected with the marker data; that is, the profiles were corrected for any displacement (bending) of the glass slide. In Figure 2a, therefore, the lower side of the base coat, that is, the interface between glass and base coat is a real, fixed reference position. The variation of the marker position in time is discussed separately later. The thick solid line in Figure 2a represents the signal profile of the dry sample. The different signal levels in the base coat and the top coat are due to signal loss, which can be explained with the help of eq 2.

Figure 2a shows the profiles during a water uptake experiment. The time between two subsequent profiles is 40 min for the first 10 profiles and 4 h for the later ones. The measurement time of a single profile is 20 min. The signal of the water on top of the coating is lower than the signal in the base coat, which is due to the fact that the $T_1$ of pure water is much longer than the chosen repetition time. (See eq 2.)

During water uptake, a signal increase is observed in the base coat layer. Because $T_1$ values are the same for dry and wet base coats (Table 2), there is no change in $T_1$ weighing of the signal during water uptake. Therefore, the signal increase can be attributed to an ingress of water into the coating and to an increase in the coating background signal (i.e., signal of the polymer of the coating). An increase in the background signal can be caused by an increase in the $T_2$ of the polymer matrix due to mobilization of the polymer.

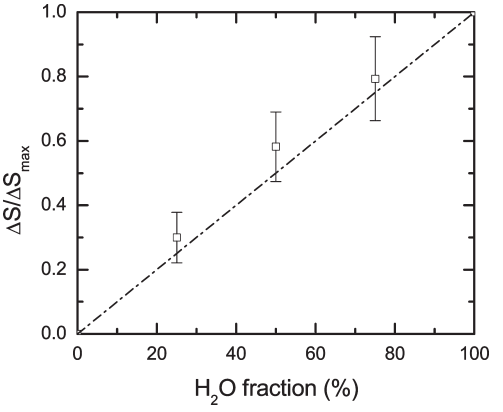


**Figure 3.** Normalized signal increase in the base coat layer as a function of the volume percentage of water in the $H_2O/D_2O$ mixture on top of the sample.

To detect changes in the background signal of the coating, the uptake of heavy water by the same type of sample was measured for 96 h. Because deuterium is not probed, only the background signal from the coating is measured. It is known that in most polymers, heavy water transport is similar to water transport.[23,24] The measured signal profiles for heavy water uptake are presented in Figure 2b. The time between two subsequent profiles is 40 min for the first 10 profiles and 4 h for the later ones. The signal level of the base coat filled with $D_2O$ is lower than the signal level of the dry base coat. Because of the swelling of the coating, the hydrogen density of the polymeric material slightly decreases, resulting in a lower signal level. Because a signal increase is not observed, it is concluded that during water uptake the observed signal increase is only due to an increase in the amount of water in the base coat layer.

The water on top of the wetted sample was replaced by various $D_2O/H_2O$ mixtures to find a relation between the signal increase and the amount of water in the base coat. The signal was integrated from the base coat/glass interface to the top coat/water interface. In Figure 3, the NMR signal is plotted against the fraction of water in the mixture on top of the sample. The normalized integrated signal change is calculated according to $\Delta S/\Delta S_{max} = [S_{mix} - S_{D_2O}]/[S_{H_2O} - S_{D_2O}]$, where $S_{mix}$, $S_{H_2O}$, and $S_{D_2O}$ are the levels of the integrated signal of the base coat layer in the case of exposure to a $D_2O/H_2O$ mixture, pure water or pure heavy water,

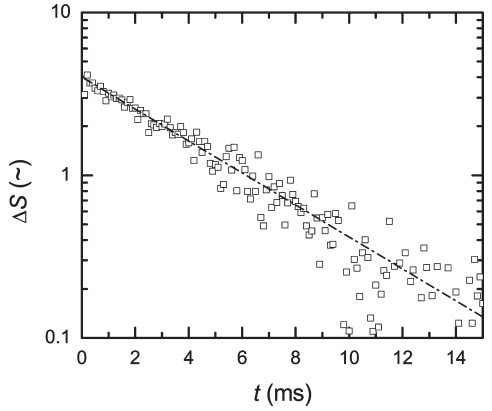


**Figure 4.** Signal decay of water in the base coat. The value of the $T_2$ relaxation time is 4.8 ms.

respectively. A linear relation between the signal and the amount of water in the mixture is observed. It can be concluded that signal increase $\Delta S$ is proportional to the mass of water in the coating $\Delta m$ (mg), $\Delta S = k\Delta m$, where $k$ ($mg^{-1}$) is a proportionality coefficient.

To quantify the signal increase, $\Delta S$, in terms of the amount of absorbed water the coefficient, $k$, should be found. The expression for $k$ can be derived by the integration of eq 2

$$k = \frac{1}{\rho_w A}[1 - \exp(-t_r/T_1)]\exp(-t_e/T_2) \qquad (3)$$

where $\Delta m$ (mg) is the amount of water in the coating, $\rho_w$ (mg/$cm^3$) is the density of liquid water, $A$ ($m^2$) is the area of the base coat, $T_1$ (s) is the longitudinal relaxation time, and $T_2$ (s) is transversal relaxation time of water. The signal loss in the wet base coat due to the $T_1$ relaxation is equal to 8% with $t_r = 0.5$ s. To estimate the signal loss of water due to $T_2$ relaxation, the signal decay of the whole base coat saturated with $D_2O$ was subtracted from the signal decay of the wet base coat. (See Figure 4.) The $T_2$ value of water in the base coat appears to be 4.8 ms. Therefore, only 2% of the signal is lost as a result of $T_2$ relaxation with used echo time, $t_e = 100$ $\mu$s. Because the signal loss due to relaxation processes is limited, eq 3 can be approximated by

$$k \approx \frac{1}{\rho_w A} \qquad (4)$$

As a check, NMR and gravimetric determination of the absorbed amount of water were compared for samples BC38/TC23E and BC38/TC23S, respectively. First, the initial mass of the dry sample was determined. Second, NMR profiles of a sample with water on top were measured. Hereafter, the water was removed, and the overall mass was measured. Subsequently, again water was placed on the sample and profiles were measured. This procedure was repeated until the end of the uptake process. In Figure 5, the mass increases in the samples are plotted as a function of total signal increase in the base coat. Because the amount of water in the top coat layer is a small fraction of the water ($\Delta m \leq 0.2$ mg) inside the total coating, this Figure reflects the amount of water in the base coat layer. The amount of water obtained by gravimetry relates linearly to the amount of water obtained with NMR. A linear fit gives the area of distribution of water, which appears to be 2.6 ($cm^2$). This value is approximately equal to the area of the studied samples.

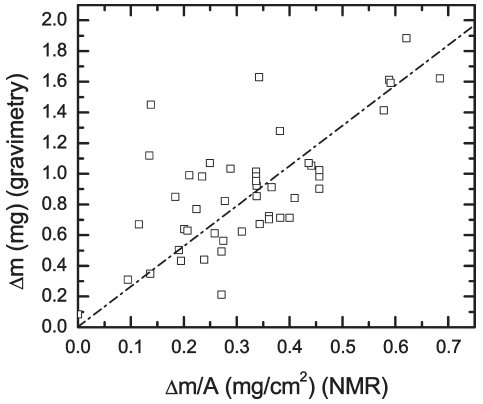


**Figure 5.** Mass change of the sample BC38/TC23E and BC38TC23S obtained on the basis of gravimetry as a function of the amount of water in the sample obtained by NMR imaging during an uptake experiment. The slope of the curve is equal to the area of the coating, $A \simeq 2.6$ $cm^2$.

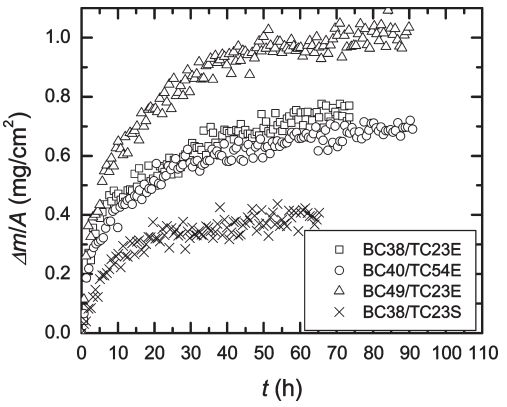


**Figure 6.** Amount of water in the base coat as a function of time during water uptake as obtained with NMR.

**Water Uptake Process.** Now the origin of the signal has been established, the water uptake process itself can be investigated. The uptake and the resulting mechanical response of the whole system will be discussed in this section.

Shortly after exposure to water, profiles show that the water is visible near the glass/base coat layer interface. (See Figure 2a.) This means that redistribution of water inside the base coat layer is faster than a single profile measurement. Moreover, it also implies that the water uptake rate is only limited by the penetration through the top coat layer. As a consequence, the total amount of water in the base coat layer is the main variable, which should be considered to characterize water uptake.

The total amount of water, $m(t)$, inside the base coat layer is obtained via integrating the profiles from the BC/glass to the TC/water interface because the top layer hardly absorbs any water. The swelling, $\Delta H(t)$, is obtained as the change in distance between the top coat/water interface and the marker from profiles measured with $t_e = 200$ $\mu$s. Because the top coat absorbs only a small amount of water, the swelling is attributed to the base coat layer. The amount of water in the base coat layer as well as the thickness change of the coating are plotted as functions of time in Figures 6 and 7, respectively.

The relation between the amount of water in the base coat and its swelling of the sample is presented in Figure 8, showing that the thickness varies linearly with the mass. Because the volume change of the base coat can be approximated with $\Delta V = A\Delta H$ ($A$ is the area of the base coat layer), it can be concluded that the molar volume of water in the

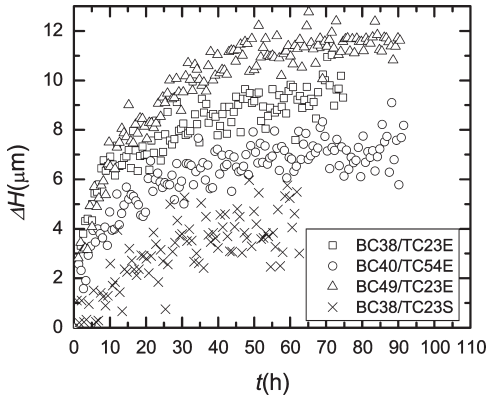


**Figure 7.** Swelling of the base coat during water uptake.

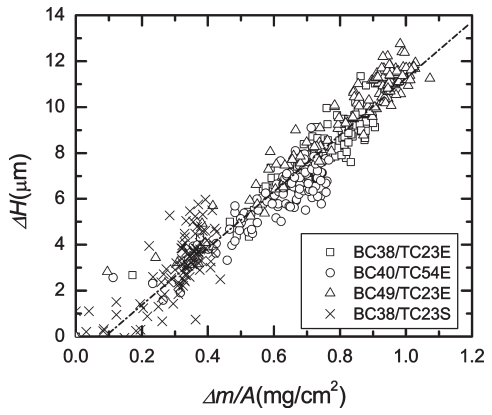


**Figure 8.** Swelling of the base coat (i.e., thickness change) as a function of the amount of water in the base coat during water uptake. The linear relation indicates that the molar volume of water inside the base coat layer is constant.

base coat layer is constant. A linear fit gives a slope $A\Delta H/\Delta m \simeq 0.2 \times 10^{-3}$ cm$^3$/mg. With the area of the base coat, obtained in the previous section, the molar volume of water $v = MA\Delta H/\Delta m$ in the base coat is estimated to be 22 cm$^3$/mol. This value is similar to the molar volume of liquid water.

Water uptake of the samples with applied external stress (BC38/TC23E, BC40/TC54E, and BC49/TC23E) initially occurs at a high rate and slows down later. The end levels of the amount of water in the coating are approximately proportional to the base coat thicknesses. This observation indicates that the base coat volume plays a role as a water reservoir. A significant deflection of the marker downward was also observed for these samples. (See Figure 9.) The similarity in behavior of the marker for all of these samples indicates that the evolution of the applied stress is the same for these samples.

In the case of the sample BC38/TC23S water uptake occurs without applied stress. No significant marker motion was observed for this sample. There are major differences in the water uptake process of this sample and sample BC38/TC23E. Note that these samples are similar, and the only difference is the glue used to fixate the tubes on top of these samples. First, the initial rate of uptake by sample BC38/TC23S is slow in comparison with uptake rate of BC38/TC23E. Second, sample BC38/TC23S absorbs approximately twice less water than BC38/TC23E. The only difference between these two samples is the external stress, which causes the difference in the water uptake processes by the samples.

**Model Ingredients.** For further interpretation of the observed features of the water uptake process, a deeper model-based analysis is needed.

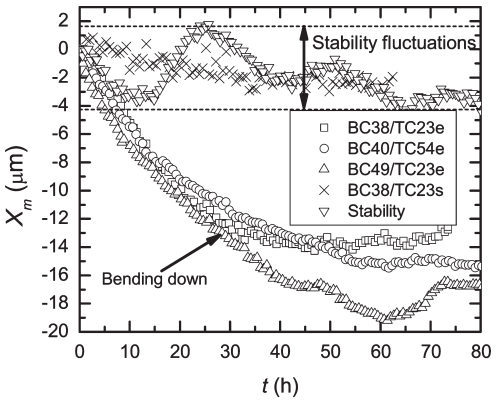


**Figure 9.** Marker position, $X_m$, during water uptake experiments for samples with epoxy-amine and silicon glues. $X_m < 0$ is a downward displacement. The deflection of the marker downward indicates a mechanical response of the sample during uptake.

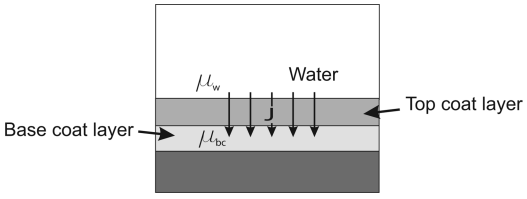


**Figure 10.** Scheme of the two-layered system with water on top of it. The water penetration into the base coat layer through the top coat layer is driven by the chemical potential difference, $\mu_{bc} - \mu_w$.

Because the amount of water in the top coat layer is low (≤0.2 mg), the water uptake process can be described as water transport to the base layer through the top layer barrier. The top coat acts as a barrier. (See the schematic picture in Figure 10.)

The water flux in the top layer can be described by Fick's law

$$J = \frac{D}{L}[\rho_0 - \rho_1] \tag{5}$$

where $D$ (m$^2$/s) is the diffusivity of water in the top coat, $L$ (m) is the thickness of the top coat layer, and $\rho_{0,1}$ (mol/m$^3$]) are the molar densities of water in the top coat layer near the interfaces with water and base coat layer, respectively. The molar density of water in the top coat is related to the chemical potential as

$$\mu_{0,1} = \mu^+ + RT \ln \rho_{0,1} \tag{6}$$

where $\mu^+$ (J/mol) is the reference chemical potential and $\mu_{0,1}$ (J/mol) is the chemical potential near the interfaces with water and base coat layer.[25] Because the chemical potential is continuous in space, $\mu_0 = \mu_w$ and $\mu_1 = \mu_{bc}$, where $\mu_w$ and $\mu_{bc}$ are the chemical potentials in water and base coat, respectively. By combining eqs 5 and 6 and using these boundary conditions, the flux can be rewritten as

$$J = \frac{D\rho_s}{L}\left[1 - \exp\left(\frac{\mu_{bc} - \mu_w}{RT}\right)\right] \tag{7}$$

where $\rho_s$ (mol/m$^3$) is water solubility in the top layer. The difference of the chemical potentials includes the osmotic pressure and the mechanical stresses in the system. The applied external stress, internal stresses in the coating, and the elastic response of the top coat on swelling contribute to

the mechanical stresses in the sample. The driving force for the transport of water through the top coat layer to the base coat layer is determined by the difference of the chemical potentials of bulk water, $\mu_w$, and water in the base coat layer, $\mu_{bc}$. Because it was shown in the previous section that the water in the base coat layer is distributed instantaneously, $\mu_{bc}$ is assumed to be constant throughout the base coat layer.

The rate of change of the amount of water in the base coat is described by

$$\frac{dn}{dt} = A'J \tag{8}$$

where $n$ (mol) is the amount of water inside the coating, $A'$ ($m^2$) is the area of the tube and $J$ (mol/$m^2$·s) is the molar flux through the top coat.

By combining the eqs 7 and 8, we can derive the following expression for water uptake

$$\frac{dn/n_{max}}{dt} = \frac{1}{\tau}\left[1 - \exp\left(\frac{\mu_{bc} - \mu_w}{RT}\right)\right] \tag{9}$$

where the time scale

$$\tau = \frac{Ln_{max}}{A'D\rho_s} \tag{10}$$

reflects the barrier properties of the top coat and the uptake capacity of the base coat. The difference of the chemical potentials, $\mu_{bc} - \mu_w$, that determines the driving force for the water uptake can be written as

$$\mu_{bc} - \mu_w = -\nu(\pi - \Delta p) \equiv -\nu P \tag{11}$$

where $\nu$ ($m^3$/mol) is the molar volume of water in the base coat, $\pi$ (Pa) is the osmotic pressure of water in the base coat, $\Delta p$ (Pa) is the excess pressure due to mechanical stresses, and $P \equiv \pi - \Delta p$ is a combination of osmotic pressure and mechanical stresses. In the previous section, it was shown that the molar volume, $v$, is constant during uptake. (See Figure 8.) Therefore, the pressures $\pi$ and $\Delta p$ drive the water uptake process.

Because distinguishing the osmotic pressure, $\pi$, and the pressure, $\Delta p$, requires detailed knowledge of the mechanical stresses in the system and the osmotic pressure, these two parameters will be represented in the pressure, $P$.

The model shows that the barrier properties of the top layer and the pressure, $P$, are needed to understand the water uptake process. A profound discussion of both the barrier properties, reflected by $\tau$, and the driving forces, represented by $P$, will be given in the next sections.

**Barrier Properties of the Top Coat Layer.** The key parameter for barrier properties, that is, $D$, cannot be estimated on the basis of the water uptake experiment, because the driving force is unknown. An estimation of the diffusivity can be obtained using a $D_2O/H_2O$ exchange experiment that is based on exchange of $D_2O$ in a saturated coating with $H_2O$. Because this process is not accompanied by a mechanical response and change in the state of the polymer matrix, the exchange rate is only determined by the diffusivity of $H_2O$ and $D_2O$ molecules in the top coat layer.

Exchange experiments have been performed on all samples. Because during water uptake the redistribution of $D_2O$ and $H_2O$ in the base coat is faster than the temporal resolution in the experiment, the exchange rate is completely determined by the rate of diffusion through the top coat layer. Figure 11 shows the decrease in the water content in the base coat $|\Delta m/A|$ as a function of time, where $\Delta m = m(t) - m_{max}$.

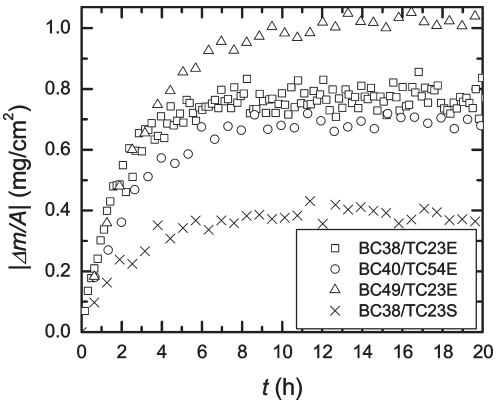


**Figure 11.** Amount of water released by the base coat layer when water is exchanged with heavy water on top of the sample in a $D_2O/H_2O$ exchange experiment.

To describe the $D_2O/H_2O$ exchange process, it was assumed that heavy water and water diffuse through the top coat layer identically.[23,24] Furthermore, the density of water above the top coat is assumed to be zero because there is an infinite reservoir of heavy water on top of the coating. Also, it was assumed that initially the coating is fully saturated with water.

The diffusion of water from the base coat through the top coat in this case was described with eqs 7 and 8 and $\rho_0 = 0$

$$\frac{dn}{dt} = -\frac{A'D}{L}\rho_1 \tag{12}$$

where $n$ (mol) is the amount of water in the base coat and $\rho_1$ (mol/$m^3$) is the density of water in the top coat at the base coat/top coat interface.

The density of water in the top coat near the interface with the base coat was assumed to be coupled to the amount of water in the base coat as $\rho_1/\rho_s = n/n_{max}$, where $n_{max}$ (mol) is the initial amount of water in the base coat and $\rho_s$ is the solubility of water in the top coat. Consequently, eq 12 can be rewritten as

$$\frac{d(n/n_{max})}{dt} = -\frac{A'D\rho_s}{Ln_{max}}n/n_{max} \tag{13}$$

The solution for this equation is

$$n \equiv n_{max}\exp\left(-\frac{t}{\tau}\right) \tag{14}$$

where $\tau \equiv Ln_{max}/A'D\rho_s$. Note that the time scale, $\tau$, of the exchange equals the time scale in eq 10.

The values $\tau$ of the exchange processes were obtained by fitting the data with eq 14 and are presented in the Table 3 together with estimates for the diffusion coefficients of water in the top coat.

The estimated value of water diffusivity in the wet top coat is approximately $D \approx 10^{-12}$ $m^2$/s, which is in agreement with reported values of water diffusivity in cross-linked coatings below the glass-transition temperature.[4]

Figure 12 shows a significant difference between rates of water uptake and $D_2O/H_2O$ exchange. This difference can be explained by the fact that the exchange process is only driven by diffusion of water through the top coat, whereas in the

**Table 3. Typical Time Scales of the $D_2O/H_2O$ Exchange Processes and the Diffusion Constants of Water in the Top Coat**

| sample | $\tau$ (h) | $D \times 10^{-12}$ ($m^2/s$) |
|---|---|---|
| BC38/TC23E | $1.9 \pm 0.1$ | $3.1 \pm 1.1$ |
| BC40/TC54E | $2.5 \pm 0.2$ | $4.3 \pm 2.2$ |
| BC49/TC23E | $3 \pm 0.1$ | $2.6 \pm 0.7$ |
| BC38/TC23S | $2.2 \pm 0.2$ | $1.5 \pm 0.7$ |

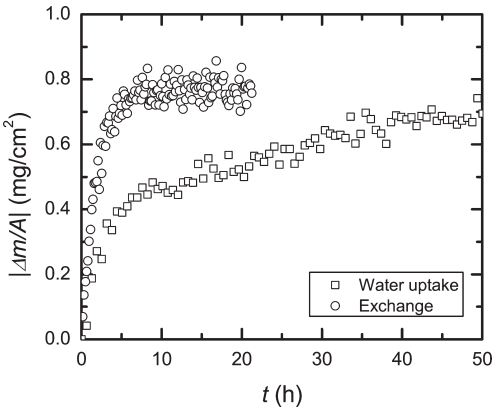


**Figure 12.** Amount of water as a function of time in the uptake and exchange experiments for the sample BC38/TC23E.

uptake experiment, the penetration of water was also driven by the evolution of $P \equiv \pi - \Delta p$.

**Driving Force and Mechanical Stress.** This section focuses on the effects of mechanical stresses on the driving force, $P$, the rate of water uptake, and the total amount of water that is absorbed by the coating.

To derive the evolution of $P \equiv \pi - \Delta p$ from the water uptake experimental data, eqs 9 and 11 were combined, resulting in

$$P = -\frac{RT}{v}\ln\left(1 - \tau\frac{\mathrm{d}n/n_{\max}}{\mathrm{d}t}\right) \qquad (15)$$

Because $n/n_{\max} = \Delta m/\Delta m_{\max}$, the pressure, $P$, can easily be extracted from eq 15. To obtain $P$, the uptake data shown in Figure 6 were fitted with the two-exponential function for the samples BC38TC23E, BC40TC54E, and BC49TC23E and with a monoexponential function for BC38TC23S. These fits were used in eq 15. Figure 13 shows $P$ as a function of $\Delta m/AH$, where $H \equiv H_0 + \Delta H$ is the total thickness of the base coat layer. Note that the variable $\Delta m/AH$ represents the average concentration of water in the base coat.

It is expected that $\Delta p$ consists of (a) internal stresses due to curing and solvent evaporation and additionally to water, (b) elastic stress generated by the top coat as a response to swelling of the base coat, and (c) the externally applied stress, which is present in all samples except the sample prepared with silicone glue. Because initially internal and elastic stresses are absent, the initial value of $P \simeq 0.01$ GPa for sample BC38/TC23S equals the initial value of the osmotic pressure $\pi_0$ of water in the base coat. (See eq 11.) For samples prepared with epoxy-amine glue, initially $P \simeq 0.1$ GPa, indicating the importance of external stress.

The typical time scale for the initial rate, $R_0$, of water uptake can be estimated from eq 9

$$R_0 = \left(\frac{\mathrm{d}n/n_{\max}}{\mathrm{d}t}\right)_{t=0} = \tau^{-1}[1 - \exp(-vP/RT)]_{t=0} \qquad (16)$$

It was observed that in the samples glued with epoxy-amine initially $vP/RT \approx 1$, meaning that the initial rate of water uptake $R_0$ is $\sim 0.6\tau^{-1}$. In the case of sample BC38/TC23S, it was observed that initially $vP/RT \approx 0.1$. In this case, the initial water uptake rate is slower, $R_0 \approx 0.1\tau^{-1}$. This difference in the initial rates is clearly visible in Figure 6. The conclusion is that the applied external stress accelerates the water uptake process.

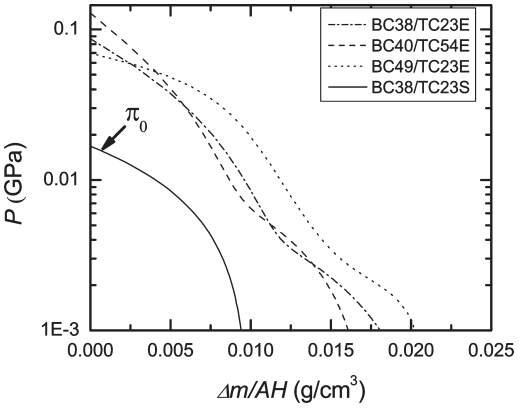


**Figure 13.** Excess pressure $P \equiv \pi - \Delta p$ in the base coat as a function of the average water concentration in the coating during water uptake. Note that $H \equiv H_0 + \Delta H(t)$ is the total thickness of the base coat. The pressure, $P$, represents the driving force of water uptake. $\pi_0$ is an initial value of the osmotic pressure in the base coat.

Another contribution of external stress is the observed fact that to achieve the equilibrium situation, the sample should take more water to compensate the applied stress, as is seen in Figure 13.

## Conclusions

High-resolution NMR imaging is the only experimental technique, which can simultaneously measure the distribution of water in multilayer coatings, the swelling, and the mechanical behavior of the complete sample during water uptake.

The rate of water penetration into a waterborne base coat is limited only by the penetration through the protective top coat layer. The penetrated water causes swelling, which appears to be linear with the total amount of absorbed water, implying that the molar volume of water in the polymer matrix of the base coat is constant and has a value that is similar to the molar volume of liquid water. It is also observed that the applied external stress increases both the uptake rate and the total amount of absorbed water.

A thermodynamical model has been formulated to serve as a guide for the interpretation of the experimental results. The model incorporates the barrier properties and the uptake driving force, reflected by diffusivity of water in the top coat and difference in chemical potentials, respectively. The diffusivity of water in the top coat has been estimated on the basis of $D_2O/H_2O$ exchange experiments and is on the order of $10^{-12}$ $m^2/s$. With the proposed model, the contribution of the applied stress to the driving force and its influence on the uptake rate have been estimated. The present study shows that mechanical stresses have a big impact on the process of water uptake by multilayer coatings.

**Acknowledgment.** The project is funded by TU/e, TNO, AkzoNobel Car Refinishes, and AkzoNobel Aerospace Coatings. We thank Hans Dalderop and Jef Noijen from TU/e for technical support and assistance, Klaas Kopinga from TU/e, Taco Scherer from AkzoNobel Car Refinishes, and Ruud van Overbeek from AkzoNobel Aerospace Coatings for discussions in sample preparation and experimental design and Kenny Raghosing from AkzoNobel Car Refinishes for samples preparation.

## References and Notes


(1) van der Wel, G. K.; Adan, O. C. G. *Prog. Org. Coat.* **1999**, *37*, 1–14.
(2) Carbonini, P.; Monetta, T.; Nicodemo, L.; Mastronardi, P.; Scatteia, B.; Belucci, F. *Prog. Org. Coat.* **1996**, *29*, 13–20.
(3) Park, J. H.; Lee, G. D.; Ooshige, H.; Nishikata, A.; Tsuru, T. *Corros. Sci.* **2003**, *45*, 1881–1894.
(4) Allahar, K. N.; Hinderliter, B. R.; Tallman, D. E.; Bierwagen, G. P. *J. Electrochem. Soc.* **2008**, *155*, F201–F208.
(5) Devasahayam, S. *J. Appl. Polym. Sci.* **2006**, *99*, 2052–2061.
(6) Fahmy, A. A.; Hurt, J. C. *Polym. Compos.* **1980**, *1*, 77–80.
(7) Weitsman, Y. *J. Mech. Phys. Solids* **1987**, *35*, 73–94.
(8) Miszczyk, A.; Schauer, T. *Prog. Org. Coat.* **2005**, *52*, 298–305.
(9) Penon, M. G.; Picken, S.; Wubbenhorst, M.; van Turnhout, J. *J. Appl. Polym. Sci.* **2007**, *105*, 1471–1479.
(10) Nguyen, T.; Byrd, E.; Bentz, D.; Lin, C. *Prog. Org. Coat.* **1996**, *27*, 181–193.
(11) Wapner, K.; Grundmeier, G. *Int. J. Adhes. Adhes.* **2004**, *24*, 193–200.
(12) Wapner, K.; Stratmann, M.; Grundmeier, G. *Electrochim. Acta* **2006**, *51*, 3303–3315.
(13) Bosch, P.; Fernandez, A.; Salvador, E. F.; Corrales, T.; Fernando, C.; Peinado, C. *Polymer* **2005**, *46*, 12200–12209.
(14) Glover, P. M.; Aptaker, P. S.; Bowler, J. R.; Ciampi, E.; McDonald, P. J. *J. Magn. Reson.* **1999**, *139*, 90–97.
(15) Erich, S. J. F.; Laven, J.; Pel, L.; Huinink, H. P.; Kopinga, K. *Prog. Org. Coat.* **2005**, *52*, 210–216.
(16) Erich, S. J. F.; Adan, O. C. G.; Pel, L.; Huinink, H. P.; Kopinga, K. *Chem. Mater.* **2006**, *18*, 4500–4504.
(17) Erich, S. J. F.; Laven, J.; Pel, L.; Huinink, H. P.; Kopinga, K. *Appl. Phys. Lett.* **2005**, *86*, 134105.
(18) Mitchell, J.; Blumler, P.; Mcdonald, P. J. *Prog. Nucl. Magn. Reson. Spectrosc.* **2006**, *48*, 161–181.
(19) McCall, D.; Douglass, D. C.; Blyler, L. L.; Johnson, G. E.; Jelinski, L. W.; Bair, H. E. *Macromolecules* **1984**, *17*, 1644–1649.
(20) Ostroff, E. D.; Waugh, J. S. *Phys. Rev. Lett.* **1966**, *16*, 1097–1099.
(21) Kopinga, K.; Pel, L. *Rev. Sci. Instrum.* **1994**, *65*, 3673–3681.
(22) Wurster, D. E.; Bhattacharjya, S.; Flanagan, D. R. *AAPS PharmSciTech* **2007**, *8*, 152–157.
(23) Popineau, S.; Rondeau-Mouro, C.; Sulpice-Gaillet, C.; Shanahan, M. *Polymer* **2005**, *46*, 10733–10740.
(24) Drew, D. W.; Clough, A. S.; Jenneson, P. M.; Shearmur, T. E.; van der Grinten, M. G. D.; Riggs, P. *Nucl. Instrum. Methods Phys. Res., Sect. B* **1996**, *119*, 429–432.
(25) Katchalsky, A.; Curran, P. F. *Nonequilibrium Thermodynamics in Biophysics*; Harvard University Press: Cambridge, MA, 1965.